Direct measurement of the protein response to an electrostatic perturbation that mimics the catalytic cycle in ketosteroid isomerase

Santosh Kumar Jha[a,1], Minbiao Ji[b,1,2], Kelly J. Gaffney[b,3], and Steven G. Boxer[a,3]

[a]Department of Chemistry, and [b]PULSE Institute, SLAC National Accelerator Laboratory, Stanford University, Stanford, CA 94305

Contributed by Steven G. Boxer, August 24, 2011 (sent for review July 12, 2011)

Understanding how electric fields and their fluctuations in the active site of enzymes affect efficient catalysis represents a critical objective of biochemical research. We have directly measured the dynamics of the electric field in the active site of a highly proficient enzyme, Δ^5-3-ketosteroid isomerase (KSI), in response to a sudden electrostatic perturbation that simulates the charge displacement that occurs along the KSI catalytic reaction coordinate. Photoexcitation of a fluorescent analog (coumarin 183) of the reaction intermediate mimics the change in charge distribution that occurs between the reactant and intermediate state in the steroid substrate of KSI. We measured the electrostatic response and angular dynamics of four probe dipoles in the enzyme active site by monitoring the time-resolved changes in the vibrational absorbance (IR) spectrum of a spectator thiocyanate moiety (a quantitative sensor of changes in electric field) placed at four different locations in and around the active site, using polarization-dependent transient vibrational Stark spectroscopy. The four different dipoles in the active site remain immobile and do not align to the changes in the substrate electric field. These results indicate that the active site of KSI is preorganized with respect to functionally relevant changes in electric fields.

enzyme catalysis | electrostatic preorganization | Stark effect | visible-pump IR probe | time-resolved anisotropy

Enzymes catalyze the vast majority of biochemical reactions and accelerate the rate of these reactions by many orders of magnitude compared to the uncatalyzed reactions in solution. The origins of the enormous catalytic power of enzymes are still not well understood despite enormous effort (1–6). In particular, the functional role of fast picosecond protein motions in catalysis and the dynamic nature of the transition state barrier crossing is a subject of ongoing and current debate (7–13). Theoretical studies have suggested that fast vibrations in enzymes might generate transition state conformations conducive to the chemical reaction (7, 8, 14–21), a familiar concept for reactions in ordinary solvents (22). In an alternative viewpoint, preorganization effects have been suggested to be a major contributing factor to enzyme catalysis (23–28). It has been postulated that enzymes have partially oriented dipoles of polar and charged groups in the active site that interact with electrostatic features present in the catalytic transition state more favorably than water can. Such preorganization of active site dipoles and charges has been suggested to result in a reduction in the reorganization energy and provide enormous catalytic advantage over the reaction in solution, where water molecules must rearrange in order to solvate charge rearrangements during the chemical reaction (24, 29–31). The relative merits of these opposing viewpoints remains unclear largely because of the paucity of direct experimental assessment of the key discrepancies between these alternative explanations for enzyme activity (11–13, 20, 31, 32). Furthermore, thermal motion is always present on all timescales, so the question is whether functionally relevant motions, specifically coupled to catalysis, are present.

We have directly measured the changes in mobility and orientation of probe dipoles in the active site of a highly proficient enzyme, Δ^5-3-ketosteroid isomerase (KSI) (Fig. 1*A*), in response to an electrostatic perturbation that mimics the movement of electronic charges during its catalytic cycle. KSI catalyzes the isomerization of 3-oxo-Δ^5-steroids to their Δ^4-conjugated isomers (28, 33–35) (Fig. 1*B*), enabling the isomerization reaction to occur approximately 10^{11}-fold faster than the uncatalyzed reaction. Biologically, the enzyme activity of homologues of KSI is critical for the synthesis of steroid hormones in mammals and plants (28, 36). We simulated the movement of electric charge along the reaction coordinate of KSI by the photoexcitation of a fluorescent intermediate analog, coumarin 183 (C183) (Fig. 1 *A* and *C*), which binds tightly in the active site of the enzyme (Fig. 2, Fig. S1, and *SI Text*). In earlier work, the electrostatic response of the active site was probed indirectly by measuring the time-dependent fluorescence Stokes shift of the dye in the active site (31). The solvation dynamics for the dye bound at the active site of the enzyme was found to be very different from what is observed for the same dye in water, suggesting that the active site solvating dipoles were highly restricted. In the present work, we directly measure the extent of reorganization of probe dipoles in the enzyme active site by employing polarization- and time-dependent IR spectroscopy (time-resolved UV-pump IR-probe spectroscopy) (37–39), as an ultrafast probe of solvation dynamics. This spectroscopic method combines the subpicosecond time resolution of the optical laser pulses with atomic level structural sensitivity of vibrational spectroscopy. Four cysteines modified with spectator thiocyanate at strategic locations in the active site (Fig. 1*A*) served as the quantitative reporter of changes in electric field and dynamics. Following the initial vibrational Stark shift resulting from the optically induced instantaneous charge redistribution on C183, no further change in the spectator probe absorption frequency or orientation was observed for any of the four thiocyanate spectator dipoles. These observations strongly indicate that the enzyme electrostatic field does not respond dynamically to the simulated motion of charge along the reaction coordinate.

Results and Discussion

Photoexcitation of KSI-Bound C183 Simulates the Movement of Electronic Charges During the Catalytic Cycle of KSI. Understanding how light-activation of C183 simulates the movement of charge

Author contributions: S.K.J., M.J., K.J.G., and S.G.B. designed research; S.K.J. and M.J. performed research; S.K.J. and M.J. contributed new reagents/analytic tools; S.K.J., M.J., K.J.G., and S.G.B. analyzed data; and S.K.J., M.J., K.J.G., and S.G.B. wrote the paper.

The authors declare no conflict of interest.

[1]S.K.J. and M.J. contributed equally to this work.

[2]Present address: Department of Chemistry and Chemical Biology, Harvard University, Cambridge, MA 02138.

[3]To whom correspondence may be addressed. E-mail: sboxer@stanford.edu or kgaffney@slac.stanford.edu.

This article contains supporting information online at www.pnas.org/lookup/suppl/doi:10.1073/pnas.1113874108/-/DCSupplemental.

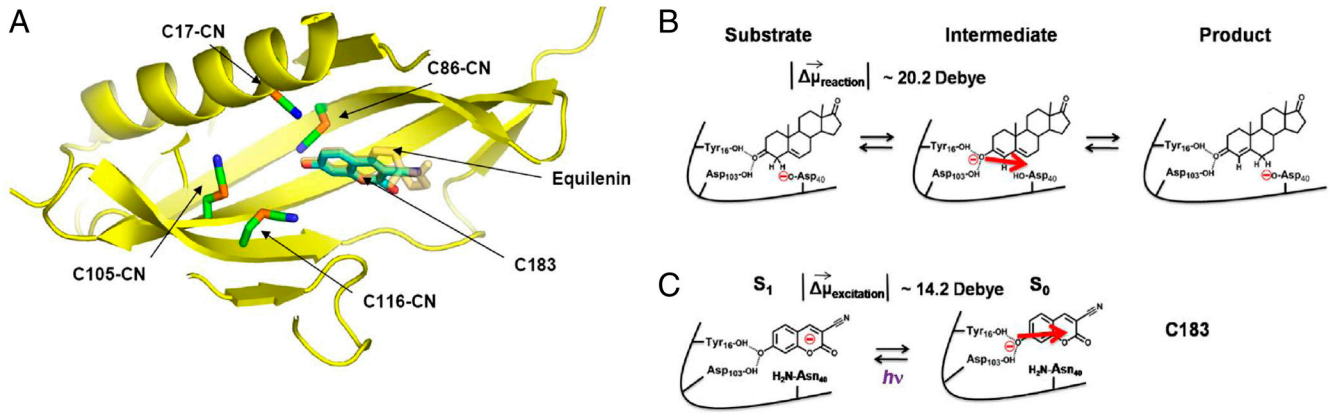

Fig. 1. Structural model of the active site of KSI bound to C183 and equilenin. (*A*) Superimposed structures of KSI variants containing a nitrile at positions 116 (C116-$^{13}C^{15}N$), 17 (C17-$^{13}C^{15}N$), 86 (C86-$^{13}C^{15}N$), or 105 (C105-$^{13}C^{15}N$) bound to equilenin (transparent yellow). C183 (blue) is aligned with equilenin in the superimposed structure. The structure was drawn from Protein Data Bank files 3OXA, 3OX9, and 3OWY using the program PyMOL. The structural model of KSI with a nitrile at position 17 (I17C-$^{13}C^{15}N$) was created using PyMOL. (*B*) The movement of electronic charge during the enzymatic reaction of KSI is compared to the movement of electronic charge during the photoexcitation of C183 (*C*). The red arrow in *B* and *C* show the direction of movement of electronic charge when moving from KSI–intermediate complex to KSI–substrate complex. An electronic difference dipole ($|\Delta\vec{\mu}_{\text{reaction}}|$) of approximately 20.2 debye is created from the movement of a single electronic charge over a distance of 4.2 Å during the passage from KSI–intermediate complex to KSI–substrate complex, which is similar in magnitude to $|\Delta\vec{\mu}_{\text{excitation}}| \sim 14.2$ debye created during photoexcitation of enzyme-bound C183 (see text).

density during the reaction catalyzed by KSI requires the consideration of the catalytic mechanism. The isomerization reaction catalyzed by KSI starts with the abstraction of an alpha proton of the steroid substrate by the negatively charged Asp40 residue of the enzyme (Fig. 1*B*). Removal of a proton leads to the formation of a dienolate intermediate where the negative charge on the oxygen atom of the carbonyl moiety is stabilized by a network of hydrogen bonds to the active site residues (Asp103, Tyr 16, Tyr57, and Tyr 32) of the enzyme (collectively referred to as the "oxyanion hole"). Hence, during the progress of the reaction from the reactant state to the intermediate state, negative charge moves toward the oxyanion hole; conversely, negative charge moves away from the oxyanion hole while proceeding from the intermediate state to the reactant state (Fig. 1*B*). From the perspective of electrostatics, the reaction is characterized by this flow of charge. In the final step of the catalytic reaction cycle, protonated Asp40 transfers its proton to the 6 position of the steroid ring to complete the reaction.

We exploit the photoacidity of a coumarin dye, C183, to simulate this movement of charge density during the reaction catalyzed by KSI, due to its structural similarity with the intermediate formed on the catalytic pathway (31). Aromatic photoacids undergo a profound change in pK_a upon photoexcitation and exhibit a lower pK_a in the photoexcited state than in the ground state (40). A charge rearrangement occurs upon photoexcitation such that electron density is transferred from the acidic functional group, often a hydroxyl group, to the aromatic ring (40, 41). Photoacidic coumarins have been used in previous studies to mimic electron and proton transfer reactions in solution (41, 42) and in the active site of KSI (31).

The strategy utilized to study the dynamical response of the active site residues of KSI along the reaction coordinate is described schematically in Fig. 1*C* (31). C183 binds tightly in the oxyanion hole (the dissociation constant of KSI-C183 binding was determined to be approximately 1.3 μM; Fig. S1*C* and *SI Text*) in the anionic form (Fig. S1*A*) and chemically resembles the intermediate state in the catalytic cycle (31, 43) (Fig. 1 *A*–*C*). The pK_a of the hydroxyl group drops from approximately 6.5 to approximately 1 upon photoexcitation (31) and charge density moves away from the deprotonated hydroxyl oxygen atom toward the aromatic ring (31, 40) (Fig. 1*C*). Thus, the photoexcited state of enzyme-bound C183 resembles the charge distribution of the reactant state of the enzyme-catalyzed reaction, because the light-activation relocates electron density away from the deprotonated hydroxyl oxygen atom and the oxyanion hole (Fig. 1 *B* and *C*).

We quantify the magnitude of electrostatic perturbation introduced by photoexcitation of C183 by measuring the difference in dipole moment of C183 between the electronic ground and excited state (electronic difference dipole, $|\Delta\vec{\mu}_{\text{excitation}}|$). We measured the electronic Stark spectrum of C183 (40) (Fig. S2, see *SI Text*), which gives a value of $|\Delta\vec{\mu}_{\text{excitation}}| = 14.2$ debye (*SI Text*, Fig. S2). In the reaction catalyzed by KSI, the movement of a single electronic charge approximately 4.2 Å from the hydroxyl atom of the dienolate intermediate to the Asp40 residue as the reaction proceeds from KSI–intermediate complex to the KSI–substrate complex (Fig. 1*B*) is expected to create a $|\Delta\vec{\mu}_{\text{reaction}}|$ of approximately 20.2 debye (one electronic charge separated by 1 Å distance creates a dipole of 4.8 debye). Hence, the magnitude of the electronic perturbation produced by photoexcitation of C183 is reasonably similar to the electronic perturbation that occurs during the reaction catalyzed by KSI, though the direction of transfer appears to be rotated by approximately 45° between the two systems.

Thiocyanate Probes Sense the Movement of Electric Charges in the Active Site of KSI. We used four different enzyme-bound spectator thiocyanate probes to study the extent of reorganization of the active site due to the change in charge distribution following the photoexcitation of C183. The vibrational frequency of the nitrile (CN) bond in a thiocyanate moiety is sensitive to its local electrostatic environment. This sensitivity to changes in the electric field manifests in a vibrational Stark shift of the CN stretch frequency given by (44, 45)

$$hc\Delta\tilde{\nu}_{\text{CN}}^{\text{obs}} = -\Delta\vec{\mu}_{\text{CN}} \bullet \Delta\vec{F} = -|\Delta\vec{\mu}_{\text{CN}}||\Delta\vec{F}|\cos\theta \qquad [1]$$

where $\Delta\tilde{\nu}_{\text{CN}}^{\text{obs}}$ is the observed difference in vibrational frequency (in inverse centimeter) of the nitrile between two different electrostatic environments, h is Planck's constant, c is the speed of light, $\Delta\vec{\mu}_{\text{CN}}$ is the change in dipole moment between the ground and excited state of the vibrational transition of the nitrile (also known as the vibrational difference dipole or Stark tuning rate, with units of inverse centimeter per megavolt per centimeter), $\Delta\vec{F}$ is the change in electric field due to photoexcitation (units of megavolt per centimeter), and θ is the angle between the nitrile probe difference dipole moment vector and the direction of the

change in the field. The direction and magnitude of $\Delta\vec{\mu}_{CN}$ have been measured for many nitrile-containing model compounds (44) as well as in proteins (46) by calibration in known applied electric fields using vibrational Stark spectroscopy. Typically, the direction of $\Delta\vec{\mu}_{CN}$ is along the nitrile-bond axis and has a magnitude of approximately 0.7 $cm^{-1}/(MV/cm)$. Because the thiocyanate probe senses the projection of the electric field change onto the nitrile-bond axis [Eq. **1**], the IR frequency shift of a thiocyanate can be quantitatively converted into electric field values if the direction of the nitrile-bond axis and its relationship to the direction of charge motion created by the photoexcitation of the enzyme-bound fluorescent ligand are known.

X-ray crystal structures of three of the probe-modified proteins used in this study (M116C-$^{13}C^{15}N$, M105C-$^{13}C^{15}N$, and F86C-$^{13}C^{15}N$) with or without the bound intermediate analog equilenin have been determined (Protein Data Bank IDs 3OXA, 3OWY, and 3OX9, respectively) (47). The structure of the fourth probe-modified protein used here (I17C-$^{13}C^{15}N$) was modeled using PyMOL (*SI Text*). An alignment of C183 with equilenin in the crystal structure of KSI (Fig. 1*A*) reveals that the four thiocyanate spectator probes are located close to the hydroxylic oxygen of the bound C183 and within a few angstroms of the polar side chains and catalytic residues in the active site, which include residues that form a network of hydrogen bonds in and around the oxyanion hole. All the four probe-modified proteins bind C183 with similar affinity (legend to Fig. S1) and the orientation of the nitrile in all the proteins is consistent with the observed vibrational Stark shift due to photoexcitation of C183 (see below and *SI Text*).

In order to more faithfully mimic the charge distribution of the KSI–dienolate intermediate complex, we used a mutant form of KSI in which Asp at position 40 in the sequence is mutated to Asn (D40N). The D40N form of KSI mimics the protonated form of the general base D40 present in the enzyme–dienolate intermediate complex (Fig. 1*B*); the oxyanion hole of KSI is negatively charged in the apo form of D40N-KSI at neutral pH (43). The negative charge is transferred to the hydroxyl oxygen of the bound ligand, in the enzyme–dienolate intermediate complex (48, 49). IR spectra of the apo and the C183-bound form of D40N-KSI (Fig. 2) reveal that the four spectator thiocyanate probes in the active site of KSI sense this movement of electric charge between the free oxyanion hole and the enzyme-bound C183 differently based upon their orientation and the distance from the deprotonated hydroxyl oxygen atom of the enzyme-bound C183. The peak vibrational frequencies of the four thiocyanate probes in the apo and the C183-bound form of the enzyme are listed in Table S1. These steady-state IR experiments show that the vibrational frequency of the nitrile bond of the KSI-bound thiocyanates is sensitive to the changes in electrostatic environment in the active site of KSI.

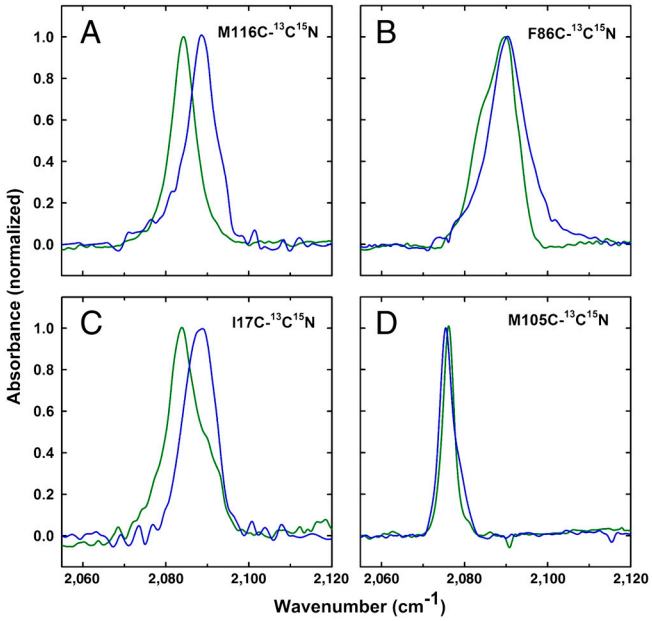

Fig. 2. Steady-state FTIR spectra of $^{13}C^{15}N$-labeled mutant forms of KSI. In each panel, the green and blue spectra denote the absorption frequency of $-^{13}C^{15}N$ attached to the sole thiol of the indicated mutant variant of KSI in the apo form and in C183 bound form, respectively.

Spectator Probe Dipoles in the KSI Active Site Do Not Change Their Energy and Orientation in Response to Electrostatic Perturbation Mimicking the Catalytic Cycle of KSI. A clear distinction between a preorganized active site versus a mechanism of enzyme catalysis which relies on ultrafast dynamic fluctuations of the active site residues for efficient catalysis requires direct measurement of the response of dipoles in the enzyme's active site as it moves along the catalytic reaction coordinate. Fig. 3 shows how the four different nitrile dipoles strategically deployed in KSI's active site respond to changes in electrostatic environment upon photoexcitation of enzyme-bound C183 (also see *SI Text* and Fig. S3). The transient IR spectra show the generation of bleach signals at 2,088.3 , 2,090.1, and 2,088.1 cm^{-1}, respectively, for the nitrile moiety placed at positions C116 (C116-$^{13}C^{15}N$), C86 (C86-$^{13}C^{15}N$), and C17 (C17-$^{13}C^{15}N$) in the active site of KSI (in proteins M116C-$^{13}C^{15}N$, F86C-$^{13}C^{15}N$, and I17C-$^{13}C^{15}N$, respectively) (Fig. 3 *A–C* and Table 1), which are directly correlated with the peak positions when C183 is bound in the active site and is in its electronic ground state (Fig. 2 and Table S1). These frequencies can be taken as the characteristic vibrational frequencies of the nitrile dipoles in the "intermediate state-like" electrostatic environment (Fig. 1 *B* and *C*). The photoexcited state of the enzyme-bound C183 is sensed by enzyme-bound nitriles as a red shift (a Stark shift) in their vibrational peaks from 2,088.3 to 2,083.3 cm^{-1} for C116-$^{13}C^{15}N$, 2,090.1 to 2,085.9 cm^{-1}

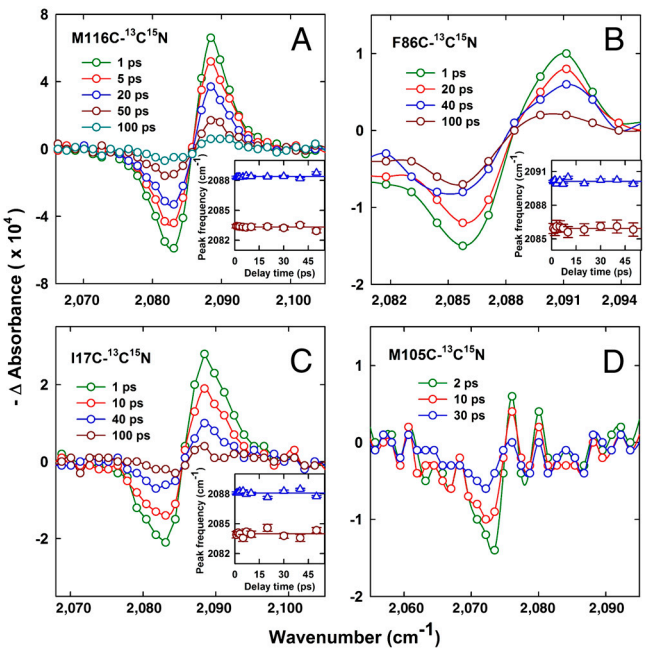

Fig. 3. Time-resolved transient IR absorption spectra of $^{13}C^{15}N$-labeled mutant forms of KSI after the photoexcitation of bound C183 at 400 nm. *A–C, Inset*, shows the mean IR-absorption frequency of $-^{13}C^{15}N$ attached to the sole thiol of the indicated mutant form of KSI, at different times after the photoexcitation of the enzyme-bound C183, in ground-state bleach (blue triangles) and electronic excited state (dark-red circles). The solid blue and red line through the data in the inset is a fit to a straight line equation.

Table 1. Mean vibrational frequencies for nitrile-modified KSI-D40N in electronic ground and excited states at pH 7.2, as determined from fitting the transient IR spectra to a sum of two pseudovoigt functions

Probe location	$\bar{\nu}_{CN}$, cm^{-1}		$\Delta\bar{\nu}_{CN}^{obs}$, cm^{-1}
	Electronic ground state	Electronic excited state	
C116-$^{13}C^{15}N$	2,088.3	2,083.3	−5
C86-$^{13}C^{15}N$	2,090.1	2,085.9	−4.2
C17-$^{13}C^{15}N$	2,088.1	2,084.0	−4.1
C105-$^{13}C^{15}N$*	—	—	—

*Due to poor signal-to-noise ratio, a precise value of frequencies could not be extracted for this position.

for C86-$^{13}C^{15}N$, 2,088.1 to 2,084.0 cm^{-1} for C17-$^{13}C^{15}N$, and too small to measure reliably for C105-$^{13}C^{15}N$ (Fig. 3, Table 1, and *SI Text*). Thus, 2,083.3, 2,085.9, and 2084.0 cm^{-1} can be taken as the characteristic vibrational frequency of C116-$^{13}C^{15}N$, C86-$^{13}C^{15}N$, and C17-$^{13}C^{15}N$, respectively, in the "reactant state-like" electrostatic environment (Fig. 1 *B* and *C*). Note that the signal-to-noise ratio of the transient IR spectra for the nitrile moiety placed at position C105 (C105-$^{13}C^{15}N$) (in protein M105C-$^{13}C^{15}N$) is very poor (Fig. 3*D*) because the nitrile dipole is nearly perpendicular to the plane of the C183 dye (see below).

The vibrational difference dipoles in C116-$^{13}C^{15}N$, C86-$^{13}C^{15}N$, and C17-$^{13}C^{15}N$ sense the change in electric field due to photoexcitation of C183 as a red shift of 5.0, 4.2, and 4.1 cm^{-1}, respectively, in the vibrational frequency (Table 1). We used a simple electrostatic model (*SI Text* and Fig. S4) based upon the energy of a dipole in an electric field to estimate these vibrational Stark shifts. The directions of the nitrile probes in the protein structure and their orientations with respect to the bound C183 are known (Fig. 1*A*, see *SI Text*). We calculated the projection of the change in electric field ($\Delta\vec{F}$) created by the electronic difference dipole of C183 on the axis of the nitrile bonds of the thiocyanate probes to extract the expected vibrational Stark shifts experienced by the vibrational dipoles (the details of modeling are discussed in *SI Text*). The vibrational Stark shifts calculated using this simple electrostatic model match the experimental Stark shifts remarkably well (Table S2). Hence, the results of this geometric analysis provide a self-consistent validation of the structural model presented in Fig. 1*A*. This simple electrostatic model also explains the poor sensitivity of C105-$^{13}C^{15}N$ as the nitrile probe is nearly perpendicular to the C183 ring (see Fig. 1*A*, the model presented in *SI Text* and Table S2). Although C105-$^{13}C^{15}N$ is less sensitive to the changes in electrostatics due to the movement of charges on the plane of C183 aromatic rings, this observation provides an additional geometrical control for the structural model presented in Fig. 1*A*. These results also indicate that the shift in vibrational frequency of enzyme-bound thiocyanates upon photoexcitation of C183 results largely from an electrostatic effect. As expected for the change in IR signal due to the Stark effect, the transient IR signals of thiocyanates in the electronic excited state of KSI-bound C183, decay with a time-constant of 31 ± 3 ps (Fig. S5), which is similar to the fluorescence lifetime of KSI-bound C183 (31).

IR spectra taken at different times after photoexcitation of enzyme-bound C183 show no further shift in IR frequency (Fig. 3 *A–C*, *Insets*); only a decay in the intensity of the difference spectrum as the excited state decays back to the ground state is observed. This result is important because if the enzyme responds dynamically to the charge perturbation that simulates the flow of electric charges along the reaction coordinate, then the vibrational frequency of the thiocyanate reporters are expected to change continuously after photoexcitation, as in a classical solvation response generally measured with electronic spectroscopy (50, 51), but also resolvable with vibrational transitions (39, 52–54). The time-independence of the nitrile stretching frequency on the picosecond timescale of three different active site dipoles, C116-$^{13}C^{15}N$, C86-$^{13}C^{15}N$, and C17-$^{13}C^{15}N$, strongly indicates that the enzyme electric field does not evolve or reorganize in response to the photoanalog of the electrostatic differences between the reactant and the intermediate state.

Polarization-dependent UV-pump IR-probe spectroscopy provides insight into the relative angles between the optical and IR-transition dipole moments (37, 38, 55). By monitoring IR signals $\Delta A_{\parallel}$ and $\Delta A_{\perp}$ when the polarizations of optical-pump and IR-probe beams are, respectively, parallel and perpendicular to each other, an anisotropy γ can be calculated which is related to the angle ϕ between the dye's optical- and the probe's IR-transition dipole moments as (42)

$$\gamma = \frac{\Delta A_{\parallel} - \Delta A_{\perp}}{\Delta A_{\parallel} + 2\Delta A_{\perp}} = \frac{3\langle\cos^2\phi\rangle - 1}{5}, \qquad [2]$$

where $\langle\ldots\rangle$ represents an ensemble average. For the nitrile probe, both the IR-transition dipole and the difference dipole moment vectors of the vibrational transition align with the nitrile-bond axis (44). Hence, by estimating the anisotropy values, it was possible to measure the changes in angle, if any, between the nitrile-bond axis and optical transition dipole of C183—i.e., whether the nitrile probes possess sufficient orientational freedom to align with the photoinduced change in electric field.

The four nitrile probes C116-$^{13}C^{15}N$, C86-$^{13}C^{15}N$, C17-$^{13}C^{15}N$, and C105-$^{13}C^{15}N$ show different ratios of $\Delta A_{\parallel}$ and $\Delta A_{\perp}$ (Fig. 4) when C183 is in electronic ground state because of their different orientation with respect to the optical transition dipole of C183. The mean value of γ in the electronic ground state

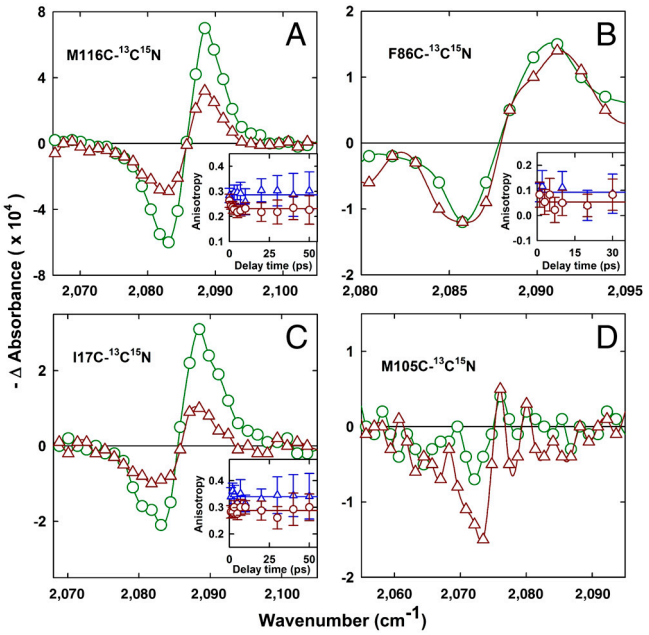

Fig. 4. Polarization-dependent transient IR absorption spectra of $^{13}C^{15}N$-labeled mutant forms of KSI at time zero. Transient spectra obtained from parallel pump and probe polarization geometries ($\Delta A_{\parallel}$) are plotted in green circles, and the spectra from perpendicular polarization geometries ($\Delta A_{\perp}$) are plotted in dark-red triangles. *A–C*, *Inset*, shows the changes in apparent anisotropy of the $^{13}C^{15}N$ attached to the sole thiol of the indicated mutant form of KSI, at different times after the photoexcitation of the enzyme-bound C183, in the ground-state bleach (blue triangles) and the electronic excited state (dark-red circles). The anisotropy was calculated using Eq. **2** with $\Delta A_{\parallel}$ and $\Delta A_{\perp}$ signals at (*A*) 2,088.3, (*B*) 2,090.1, and (*C*) 2,088.1 cm^{-1}, respectively, for the electronic ground state and at (*A*) 2,083.0, (*B*) 2,085.7, and (*C*) 2,083.7 cm^{-1}, respectively, for the electronic excited state. The solid blue and red line through the data in the insets is a fit to a straight line equation.

of C183 was determined to be 0.3 for C116-$^{13}C^{15}N$, 0.1 for C86-$^{13}C^{15}N$, and 0.32 for C17-$^{13}C^{15}N$ (Fig. 4 *A–C*, *Insets*), which corresponds to an average angle of approximately 24°, 45°, and 21° between the respective nitrile-bond axis and the optical transition dipole moment of C183. For C105-$^{13}C^{15}N$, the changes in absorption are very weak due to its poor sensitivity and it was not possible to estimate anisotropy values. Nevertheless, in this case, $\Delta A_{\perp}$ signal appears more than $\Delta A_{\parallel}$ signal (Fig. 4*D*), which conforms to the fact that C105-$^{13}C^{15}N$ is nearly perpendicular to the C183 molecular plane (Fig. 1*A*). The anisotropy values remain constant in time both when C183 is in the electronic ground state and in the electronic excited state (*SI Text*) for all the three nitrile probes, C116-$^{13}C^{15}N$, C86-$^{13}C^{15}N$, and C17-$^{13}C^{15}N$, where it was possible to calculate anisotropy values (Fig. 4 *A–C*, *Insets*). This result indicates that the angles between these three nitrile probes located in the active site and the bound C183 molecule do not change in response to the charge perturbation that simulates the flow of electric charge along the reaction coordinate of KSI.

Implications for Dynamic Theories of Barrier Crossing During Enzymatic Catalysis. Two opposing and limiting theories of enzyme catalysis revolve around the nature of mechanical and electrostatic fluctuations in the enzyme active site. In one of the theories, fast (approximately picosecond) vibrations (protein breathing modes) and a network of coupled motions within the enzyme–substrate complex have been hypothesized to be linked to transition state formation and reduction of the barrier for chemical change (10, 13, 15, 21). It has also been suggested that dynamic excursions of active site architecture on the picosecond timescale create variable electronic interactions between enzyme and reactants, which induce catalytic barrier crossing (7, 8, 10, 17, 19). In an alternative theory of enzyme catalysis, it has been proposed that electrostatic forces, due to preorganized active site dipoles and charges, primarily drive the formation of the transition state during enzymatic catalysis, and dynamic motion of the active site residues are unimportant or even deleterious (23–28, 56).

In the experiments presented in this study, we have directly measured the dynamics of different parts of the enzyme's active site on the picosecond timescale when the electronic charge distribution in the active site is changing from reactant state-like to intermediate state-like across the transition state barrier. The results show that three different dipoles in the active site of KSI do not show any time-evolving electrostatic response on the picosecond timescale or realign their dipoles to the changing electric field. For this very proficient enzyme, picosecond dynamics do not appear to be important for catalytic barrier crossing.

A recent computational study reports that Asp40 and the oxyanion hole residues of KSI undergo conformational changes during the catalytic reaction (57). Our experimental approach does not capture all aspects of KSI catalysis. Most notably, proton extraction by Asp40 during the catalytic cycle is obviously not modeled in the D40N mutant. Nevertheless, the results presented in this study combined with the results of fluorescence Stokes shift experiments in a previous study (31) strongly suggest that the solvation response of most of the active site residues at the active site is quite restricted, a behavior that is not found in typical solvents outside of proteins.

An electrostatically preorganized active site of an enzyme will not create a fluctuating electric field as the substrate reacts along the catalytic reaction coordinate. This resistance to change its electrostatic environment was observed during the light-driven reaction analog in the active site of KSI. In our study, the electrostatic response and angular mobility of the enzyme's active site dipoles have been directly measured along the catalytic reaction coordinate, a functionally relevant motion, and the results that the active site dipoles remain immobile and do not align to changes in the substrate electric field support the electrostatic preorganization model of enzyme catalysis.

Materials and Methods

Protein Expression, Purification, and Thiocyanate Labeling. The present work employs four single cysteine mutant forms of KSI in each of which the sole thiol group is chemically modified into a thiocyanate and Asp40 is mutated to Asn (D40N). All the four mutant enzymes (C69S/C81S/C97S/D40N)/M116C, (C69S/C81S/C97S/D40N)/F86C, (C69S/C81S/C97S/D40N)/I17C, and (C69S/C81S/C97S/D40N)/M105C were expressed and purified according to a previously published protocol (43). The purified enzymes were labeled with K$^{13}C^{15}N$ according to a previously published protocol (58). Isotopically labeled $-^{13}C^{15}N$ was used to shift the spectator probe frequencies as far as possible from the nitrile on C183 (see Fig. S6), an example of the advantage of this chemical labeling strategy. All four proteins were found by mass spectrometry to be >95% labeled, with an expected 27-Da increase in the mass due to the $-^{13}C^{15}N$ adduct. The fluorescence and circular dichroism spectra of all the four probe-modified proteins are similar to the wild-type KSI in both the native and unfolded states, which indicates that the gross tertiary and secondary structure of KSI is preserved across all the four probe-modified proteins. See *SI Text* for further details.

Binding Experiments Using UV-Visible Absorption and Steady-State Fluorescence. The binding of C183 with KSI was monitored with changes in UV-visible absorption spectra and steady-state fluorescence. See *SI Text* for details.

Steady-State FTIR Experiments. All the steady-state IR spectra were obtained on a Bruker Vertex 70 FTIR spectrometer equipped with an InSb detector as detailed in *SI Text*.

Electronic Stark Experiments. The magnitude of the electronic difference dipole of C183 was measured using electronic Stark spectroscopy as described in *SI Text*.

UV-Pump IR-Probe Experiments. We use subpicosecond duration 400-nm pulses to excite C183, and broadband mid-IR pulses to probe the transient spectra of the CN stretches on KSI and C183. The cross-correlation of the pump and probe pulses is less than 200 fs FWHM. A spectral resolution of approximately 1 cm^{-1} is achieved by using a spectrometer with a 32×2 mercury-cadmium-telluride array detector as detailed in *SI Text*.

Modeling of Vibrational Stark Shifts. A simple electrostatic model based upon the energy of a dipole in an electric field is used to calculate the vibrational stark shift experienced by nitriles at different locations in KSI, in response to photoexcitation of enzyme-bound C183. The model is described in *SI Text*.

ACKNOWLEDGMENTS. We thank Nick Levinson and Stephen Fried for fruitful discussions and for their critical comments on the manuscript. Plasmids containing the genes of mutant forms of KSI were graciously provided by the Herschlag Laboratory at Stanford University. We gratefully acknowledge support from the National Institutes of Health (Grant GM27738). M.J. and K.J.G. acknowledge support of the time-resolved measurements through the PULSE Institute at SLAC National Accelerator Laboratory by the US Department of Energy, Office of Basic Energy Sciences.

1. Kraut J (1988) How do enzymes work? *Science* 242:533–540.
2. Radzicka A, Wolfenden R (1995) A proficient enzyme. *Science* 267:90–93.
3. Bruice TC (2002) A view at the millennium: The efficiency of enzymatic catalysis. *Acc Chem Res* 35:139–148.
4. Kraut DA, Carroll KS, Herschlag D (2003) Challenges in enzyme mechanism and energetics. *Annu Rev Biochem* 72:517–571.
5. Zhang X, Houk KN (2005) Why enzymes are proficient catalysts: Beyond the Pauling paradigm. *Acc Chem Res* 38:379–385.
6. Frauenfelder H (2008) What determines the speed limit on enzyme catalysis? *Nat Chem Biol* 4:21–22.
7. Agarwal PK, Billeter SR, Rajagopalan PT, Benkovic SJ, Hammes-Schiffer S (2002) Network of coupled promoting motions in enzyme catalysis. *Proc Natl Acad Sci USA* 99:2794–2799.
8. Basner JE, Schwartz SD (2005) How enzyme dynamics helps catalyze a reaction in atomic detail: A transition path sampling study. *J Am Chem Soc* 127:13822–13831.
9. Olsson MH, Parson WW, Warshel A (2006) Dynamical contributions to enzyme catalysis: Critical tests of a popular hypothesis. *Chem Rev* 106:1737–1756.
10. Schwartz SD, Schramm VL (2009) Enzymatic transition states and dynamic motion in barrier crossing. *Nat Chem Biol* 5:551–558.
11. Bandaria JN, et al. (2010) Characterizing the dynamics of functionally relevant complexes of formate dehydrogenase. *Proc Natl Acad Sci USA* 107:17974–17979.

12. Chang CW, et al. (2010) Ultrafast solvation dynamics at binding and active sites of photolyases. *Proc Natl Acad Sci USA* 107:2914–2919.
13. Johannissen LO, Scrutton NS, Sutcliffe MJ (2008) The enzyme aromatic amine dehydrogenase induces a substrate conformation crucial for promoting vibration that significantly reduces the effective potential energy barrier to proton transfer. *J R Soc Interface* 5:S225–232.
14. Warshel A (1984) Dynamics of enzymatic reactions. *Proc Natl Acad Sci USA* 81:444–448.
15. Fedorov A, et al. (2001) Transition state structure of purine nucleoside phosphorylase and principles of atomic motion in enzymatic catalysis. *Biochemistry* 40:853–860.
16. Bolhuis PG, Chandler D, Dellago C, Geissler PL (2002) Transition path sampling: Throwing ropes over rough mountain passes, in the dark. *Annu Rev Phys Chem* 53:291–318.
17. Hammes-Schiffer S (2002) Impact of enzyme motion on activity. *Biochemistry* 41:13335–13343.
18. Crehuet R, Field MJ (2007) A transition path sampling study of the reaction catalyzed by the enzyme chorismate mutase. *J Phys Chem B* 111:5708–5718.
19. Saen-Oon S, Quaytman-Machleder S, Schramm VL, Schwartz SD (2008) Atomic detail of chemical transformation at the transition state of an enzymatic reaction. *Proc Natl Acad Sci USA* 105:16543–16548.
20. Bandaria JN, Dutta S, Hill SE, Kohen A, Cheatum CM (2008) Fast enzyme dynamics at the active site of formate dehydrogenase. *J Am Chem Soc* 130:22–23.
21. Ruiz-Pernia JJ, Tunon I, Moliner V, Hynes JT, Roca M (2008) Dynamic effects on reaction rates in a Michael addition catalyzed by chalcone isomerase. Beyond the frozen environment approach. *J Am Chem Soc* 130:7477–7488.
22. Chandler D (1986) Roles of classical dynamics and quantum dynamics on activated processes occurring in liquids. *J Stat Phys* 42:49–67.
23. Perutz MF (1978) Electrostatic effects in proteins. *Science* 201:1187–1191.
24. Wolfenden R (1983) Waterlogged molecules. *Science* 222:1087–1093.
25. Warshel A (1998) Electrostatic origin of the catalytic power of enzymes and the role of preorganized active sites. *J Biol Chem* 273:27035–27038.
26. Cannon WR, Benkovic SJ (1998) Solvation, reorganization energy, and biological catalysis. *J Biol Chem* 273:26257–26260.
27. Warshel A, et al. (2006) Electrostatic basis for enzyme catalysis. *Chem Rev* 106:3210–3235.
28. Feierberg I, Aqvist J (2002) The catalytic power of ketosteroid isomerase investigated by computer simulation. *Biochemistry* 41:15728–15735.
29. Warshel A, Aqvist J, Creighton S (1989) Enzymes work by solvation substitution rather than by desolvation. *Proc Natl Acad Sci USA* 86:5820–5824.
30. Olsson MH, Warshel A (2004) Solute solvent dynamics and energetics in enzyme catalysis: The S(N)2 reaction of dehalogenase as a general benchmark. *J Am Chem Soc* 126:15167–15179.
31. Childs W, Boxer SG (2010) Solvation response along the reaction coordinate in the active site of ketosteroid isomerase. *J Am Chem Soc* 132:6474–6480.
32. Wang L, Goodey NM, Benkovic SJ, Kohen A (2006) Coordinated effects of distal mutations on environmentally coupled tunneling in dihydrofolate reductase. *Proc Natl Acad Sci USA* 103:15753–15758.
33. Hawkinson DC, Eames TC, Pollack RM (1991) Energetics of 3-oxo-delta 5-steroid isomerase: source of the catalytic power of the enzyme. *Biochemistry* 30:10849–10858.
34. Ha NC, Choi G, Choi KY, Oh BH (2001) Structure and enzymology of Delta5-3-ketosteroid isomerase. *Curr Opin Struct Biol* 11:674–678.
35. Pollack RM (2004) Enzymatic mechanisms for catalysis of enolization: Ketosteroid isomerase. *Bioorg Chem* 32:341–353.
36. Oh KS, et al. (2000) Role of catalytic residues in enzymatic mechanisms of homologous ketosteroid isomerases. *Biochemistry* 39:13891–13896.
37. Moore JN, Hansen PA, Hochstrasser RM (1988) Iron-carbonyl bond geometries of carboxymyoglobin and carboxyhemoglobin in solution determined by picosecond time-resolved infrared spectroscopy. *Proc Natl Acad Sci USA* 85:5062–5066.
38. Rubtsov IV, Redmore NP, Hochstrasser RM, Therien MJ (2004) Interrogating conformationally dependent electron-transfer dynamics via ultrafast visible pump/IR probe spectroscopy. *J Am Chem Soc* 126:2684–2685.
39. Baiz CR, Kubarych KJ (2010) Ultrafast vibrational Stark-effect spectroscopy: Exploring charge-transfer reactions by directly monitoring the solvation shell response. *J Am Chem Soc* 132:12784–12785.
40. Silverman LN, Spry DB, Boxer SG, Fayer MD (2008) Charge transfer in photoacids observed by stark spectroscopy. *J Phys Chem A* 112:10244–10249.
41. Westlake BC, et al. (2011) From the cover: Concerted electron-proton transfer in the optical excitation of hydrogen-bonded dyes. *Proc Natl Acad Sci USA* 108:8554–8558.
42. Wang C, Akhremitchev B, Walker GC (1997) Femtosecond infrared and visible spectroscopy of photoinduced intermolecular electron transfer dynamics and solvent-solute reaction geometries: Coumarin 337 in dimethylaniline. *J Phys Chem A* 101:2735–2738.
43. Kraut DA, et al. (2006) Testing electrostatic complementarity in enzyme catalysis: Hydrogen bonding in the ketosteroid isomerase oxyanion hole. *PLoS Biol* 4:e99.
44. Andrews SS, Boxer SG (2000) Vibrational stark effects of nitriles I. Methods and experimental results. *J Phys Chem A* 104:11853–11863.
45. Suydam IT, Snow CD, Pande VS, Boxer SG (2006) Electric fields at the active site of an enzyme: Direct comparison of experiment with theory. *Science* 313:200–204.
46. Fafarman AT, Boxer SG (2010) Nitrile bonds as infrared probes of electrostatics in ribonuclease S. *J Phys Chem B* 114:13536–13544.
47. Fafarman AT, Sigala PA, Herschlag D, Boxer SG (2010) Decomposition of vibrational shifts of nitriles into electrostatic and hydrogen-bonding effects. *J Am Chem Soc* 132:12811–12813.
48. Childs W, Boxer SG (2010) Proton affinity of the oxyanion hole in the active site of ketosteroid isomerase. *Biochemistry* 49:2725–2731.
49. Sigala PA, Fafarman AT, Bogard PE, Boxer SG, Herschlag D (2007) Do ligand binding and solvent exclusion alter the electrostatic character within the oxyanion hole of an enzymatic active site? *J Am Chem Soc* 129:12104–12105.
50. Horng ML, Gardecki JA, Papazyan A, Maroncelli M (1995) Subpicosecond measurements of polar solvation dynamics: Coumarin 153 revisited. *J Phys Chem* 99:17311–17337.
51. Cohen BE, et al. (2002) Probing protein electrostatics with a synthetic fluorescent amino acid. *Science* 296:1700–1703.
52. Chudoba C, Nibbering ETJ, Elsaesser T (1998) Site-specific excited-state solute-solvent interactions probed by femtosecond vibrational spectroscopy. *Phys Rev Lett* 81:3010–3013.
53. Asbury JB, Wang Y, Lian T (2002) Time-dependent vibration stokes shift during solvation: Experiment and theory. *Bull Chem Soc Jpn* 75:973–983.
54. Van Tassle AJ, Prantil MA, Fleming GR (2006) Investigation of the excited state structure of DCM via ultrafast electronic pump/vibrational probe. *J Phys Chem B* 110:18989–18995.
55. Lim M, Jackson TA, Anfinrud PA (1995) Binding of CO to myoglobin from a heme pocket docking site to form nearly linear Fe-C-O. *Science* 269:962–966.
56. Warshel A (1978) Energetics of enzyme catalysis. *Proc Natl Acad Sci USA* 75:5250–5254.
57. Chakravorty DK, Hammes-Schiffer S (2010) Impact of mutation on proton transfer reactions in ketosteroid isomerase: Insights from molecular dynamics simulations. *J Am Chem Soc* 132:7549–7555.
58. Fafarman AT, Webb LJ, Chuang JI, Boxer SG (2006) Site-specific conversion of cysteine thiols into thiocyanate creates an IR probe for electric fields in proteins. *J Am Chem Soc* 128:13356–13357.